Multi-dimensional anatomical representation: A volumetric comparison of the C57BL/6 and N3 C57BL/6 x 129/Sv mouse brain modelled from serial section using Autodesk Maya

Stephen Fai[1,2], Katie Graham[1-3], Andrew J. Syrett[2,3], Brendan Trickey[3], Nico Valenzuela[1-3], and Steffany A.L. Bennett[2,3]

[1]Carleton Immersive Media Studio, Azrieli School of Architecture and Urbanism, Carleton University, Ottawa, Ontario, K1S 5B6, Canada.
{sfai, kwurts, nvalenzuela}@cims.carleton.ca
http://www.cims.carleton.ca
[2]CIHR Training Program in Neurodegenerative Lipidomics, [3]Ottawa Institute of Systems Biology, Neural Regeneration Laboratory, Department of Biochemistry, Microbiology and Immunology, University of Ottawa, Ontario, K1H 8M5, Canada.
andrew.syrett@gmail.com, btrickey@gmail.com, sbennet@uottawa.ca

Abstract. Our capacity to model human disease through genetic manipulation has made the mouse (*Mus musculus*) one of the most important entities in biomedicine. Transgenic and targeted genetic mouse models of neurodegenerative disease are typically engineered on a mixed background of inbred mouse lines, i.e., 129/Sv and C57BL/6. These inbred strains display significant neuroanatomical differences. The cerebral architecture of hybrid C57BL/6 x 129/Sv mice, however, has not been defined. Here, we describe the reconstruction of serial 5 μm paraffin-embedded, sagittal brain sections from N3 C57BL/6 x 129/Sv mice into 2D and 3D digital models. Using these datasets, we quantify the volume of various anatomical brain structures comparing N3 brains with both donor and recipient inbred strains. We further discuss how these 3D atlases can be used to map "-omic" spatial information derived from mouse models of neurodegenerative disease. Animations are freely available at http://neurolipidomics.com/resources.html.

Keywords: visualization, 3D mapping, neuroanatomy, lipidomics, bioinformatic spatial representation, genetics, mouse models.

1   Introduction

Genetic manipulation has enabled researchers to investigate the contributions of individual genes and mutations to disease progression in murine models. In neuroscience, however, these studies must take into consideration the differences in cerebral architecture that exist between inbred mice strains [1]. These innate differences complicate the analysis of hybrid transgenic animals [2]. Typically, these mice are obtained in a mixed genetic background. Of these, the 129/Sv and C57BL/6 lines are

two of the most common inbred strains used [3]. Ideally, genetically altered hybrid mice are backcrossed onto a pure genetic lineage (i.e., C57BL/6) before analysis to allow for comparisons between mutant and congenic un-manipulated "wild-types" (WTs). Backcrossing is, however, costly, labour-intensive, time-consuming, and requires a significant number of mice – it can take up to 3 years to produce congenic mice that are 99.98% genetically identical [4]. Mice must be backcrossed for 12 generations (N12) onto a recipient line (i.e., C57BL/6) to achieve this level of clonogenicity [4]. This time could be better spent (using fewer mice) assessing mutant phenotypes immediately. As such, many researchers stop backcrossing at the N3 generation, a point at which the genetically engineered colony contains a sufficient number of animals for experimental use. Hybrid N3 mice, however, have their own unique neuroanatomy (Figure 1). Published atlases of either their inbred donor (129/Sv) or recipient (C57BL/6) lineages (e.g., [1, 5-7]) cannot be used to navigate their cerebral architecture, complicating studies requiring surgical interventions. Mutant mice must be compared to genetically matched WT littermates. These WTs are generated through filial matings of each N3 line's particular heterozygote (i.e., a mouse carrying one mutant and one WT allele). Heterozygote matings produce progeny that are homozygous N3 WTs (two un-manipulated alleles), N3 heterozygote mice (one mutant and one WT allele), or homozygous N3 transgenics (two mutant alleles) at a Mendelian ratio of 1:2:1. Currently, we do not have sufficient data about the degree of interanimal variability in anatomical structure at the N3 generation nor do we have atlases that would enable surgical intervention and anatomical reference points. These resources would fundamentally accelerate evaluation of transgenic influences on cerebral development and targeted monogenic influences on disease etiology.

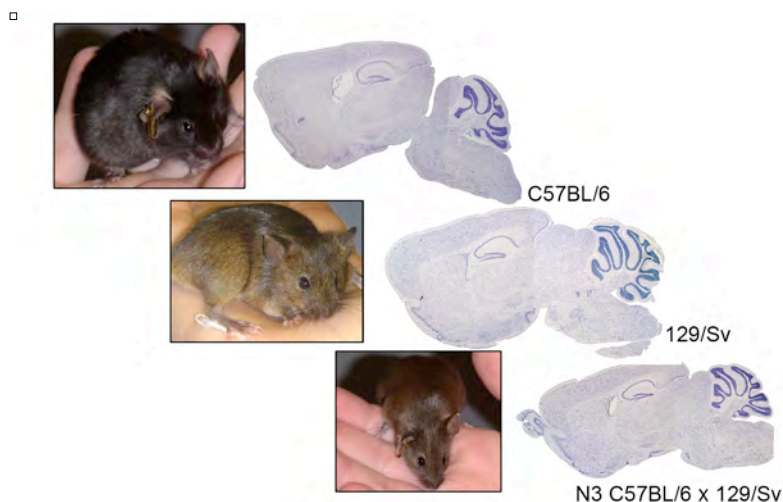Why focus efforts on the N3 C57BL/6 x 129/Sv mixed hybrid line? Multiple

Figure 1. Inbred C57BL/6 and 129/Sv mice exhibit well-defined neuroanatomical differences, clearly delineated in existing comparative 2D atlases [1, 5, 6]. N3 C57BL/6 x 129/Sv hybrids exhibit both intermediate and unique anatomical characteristics that have not been mapped.

genetic conditions can be modelled using *Mus musculus*. Because of the similarity between the human and mouse genome, and the ease with which the mouse genome can be manipulated, transgenic and targeted genetic interventions represent the most elegant means of studying genetic determinants of human disease *in vivo* [8]. The term "transgenic" gene insertion refers to the integration of foreign DNA into the host genome at random locations. Typically, fertilized C3H/HeJ x C57BL/6, FVB/N x C57BL/6, or 129/Sv x C57BL/6 oocytes are used. Different engineered lines are then assessed for degree of mutant gene expression and the effect of the positioning ectopic DNA insertion on host genome. Targeted knockout/in models take advantage of homologous recombination to either remove or replace segments of DNA directly at a target locus. "Knockover" strategies explore compensatory effects of related genes by replacing a given genetic sequence with that of a homologous family member. Combinations of transgenic and knockin models, coupled with inducible knockout methodologies, allow for production "humanized" mouse models wherein human genes replace endogenous murine sequences [9]. Finally, knockdown methodologies, wherein animals are engineered to express short hairpin RNA sequences that interfere with the transcription of target genes, can be used to mimic regionally specific genetic effects on brain function [10].

Targeted genomic insertions (i.e., knockout, knockin, knockover, knockdown strategies) begin with the integration of a single genetically altered donor embryonic stem (ES) cell, commonly a 129/Sv ES cell into a WT blastocyst, typically a C57BL/6 blastocyst. Progeny are chimeras. Some of their cells are derived from the genetically manipulated 129/Sv ES donor cells while others are derived from the C57BL/6 WT recipient cells. Chimeras are bred against inbred WT mice, again typically C57BL/6, to identify mice that have integrated the desired genetic alteration into the germline. Once germline transmission is achieved, three backcrosses (N3) are required before a sufficient number of heterozygote mice, carrying one mutant allele and one WT allele, can be obtained for filial mating and production of homozygous mutant and WT littermates. 129/Sv donor and C57BL/6 recipient lineage combinations were historically preferred for three reasons: First, 129/Sv ES cells incorporate microinjected exogenous DNA more efficiently than other ES cell lines. Second, 129/Sv ES cells maintain pluripotency more readily *in vitro*. Third, 129/Sv ES cells are more adept at competing with C57BL/6 host cells and colonizing the inner cell mass [11]. Thus, 2D reference atlases that document the degree of inter-animal variation in N3 C57BL/6 x 129/Sv hybrids would facilitate rapid analysis of changes in brain architecture representative of a majority of transgenic and targeted gene manipulation models.

What purpose do 3D hybrid neuroanatomical mouse atlases serve? We argue that a better understanding of the metabolome is key to establishing why some individuals are susceptible and other resistant to genetic determinants of neurodegenerative disease. This understanding, however, requires capacity to simultaneously visualize, analyse, and disseminate defining spatial and temporal metabolic regulatory relationships in 3D space. Excellent 3D resources are available for inbred strains [12, 13] but, to our knowledge, no 3D reconstruction of the N3 hybrid C57BL/6 x 129/Sv murine neuroanatomy exists. Here, we describe the generation of a 2D reference atlas

and a 3D model of the N3 C57BL/6 x 129/Sv WT adult male mouse. We also used this same 3D methodology to model the C57BL/6 recipient line. We quantified the volume of seven brain regions in the N3 hybrid relative to both inbred C57BL/6 and 129/Sv mice and validated 3D positioning of the hippocampus by stereotaxic injection. Finally, we discuss how these models can be used to map larger "-omic" datasets in anatomical space and over time.

2   Volumetric reconstruction of the C57BL/6 and N3 C57BL/6 x 129/Sv mouse brain

Our 2D and 3D models were reconstructed from serial 5 μm sagittal sections of paraffin-embedded, paraformaldehyde-fixed, brain tissue. Photomicrographs of cresyl violet-stained sections were registered, colour-balanced, and nine structures (exterior surface, corpus callosum, striatum, cortex, ventricles, hippocampus, dentate gyrus, CA fields of the hippocampus, granule layer of the dentate gyrus) were mapped in serial sections in Adobe Photoshop CS5. Structures were reconstructed in 3D using AutoDesk Maya 2012. An atlas mapping the cytoarchitecture of nine structures in N3 C57BL/6 X 129/Sv hybrid and an inbred C57BL/6 mice was produced. These models depict spatial differences in the neuroanatomy of N3 hybrid and C57BL/6 inbred recipient lines. Finally, from Nissl stained serial sections and extrapolated 3D models, we also obtained volumetric measurements of seven structures using the Advanced Measurement Module of OpenLab v5.0. Quantitative comparisons of strain differences and variability were obtained and this modelling approach was validated by stereotaxic injections of the retrograde tracer fluorogold.

2.1   Tissue processing

A total of 24 three-month old male animals were analyzed. N3 hybrid WT C57BL/6NCrL x 129/SvEVTac mice (n=8) were produced "in-house" from heterozygote mating of N3 F2 connexin36$^{+/-}$ mice, a kind gift of Dr David Paul (Harvard Medical School) [14]. Hybrid mice were compared to the breeder-specific inbred lines C57BL/6NCrl (n=8) and 129/SvEVTac (n=8) mice obtained from Charles River Laboratories, Saint-Constant, Quebec and Taconic Laboratories, Rensselaer, NY respectively. Mice were anesthetized by intraperitoneal injection of 5 mg/kg euthanyl (Bimeda-MTC Animal Health Ins., Cambridge, ON, Canada), and sacrificed by transcardiac perfusion with 10 mM phosphate buffered saline (PBS: 10 mM sodium phosphate and 154 mM NaCl) followed by 3.7% paraformaldehyde in PBS. All protocols were approved by the Animal Care Committee of the University of Ottawa according to guidelines set forth by the Canadian Council on Animal Care. After cardiac perfusion and before brain removal, two interaural holes were drilled laterally through the skull. Two holes were also drilled vertically at the top of the skull at bregma and lambda, scarring the surface of the brain and creating reference markers for subsequent alignment. Brains were removed, post-fixed for 24 h, and cryoprotected in 20% sucrose. Tissue was embedded in paraffin and serial 5 μm sagittal (n=2/strain, ~1780)

or coronal (n=2/strain ~4700) sections were collected on a Leica 2035 microtome. For n=18 animals, a more rapid collection protocol was employed. Successive five serial 5 μm sections were collected and 10 were discarded before re-collection (n=3/strain/orientation). Tissue sections were floated in a 42ºC water bath and mounted on Fisherbrand Superfrost/Plus glass slides. Slides were dried at 37°C overnight. Sections were deparaffinized and stained as repeating serial triads using a Leica Bond-III automated stainer with cresyl violet, hematoxylin and eosin, or luxol fast blue. Slides were mounted in resinous mounting media, and coverslipped (Fisher). Photomicrographs were obtained using a 1X objective on a Nikon Eclipse 80i light microscope equipped with a Micropublisher 5.0 RTV digital camera. The images were saved in TIFF format at a resolution of 3300 x 2550 pixels at a resolution of 300 pixels/inch with scale bars registered on each image (Figure 2).
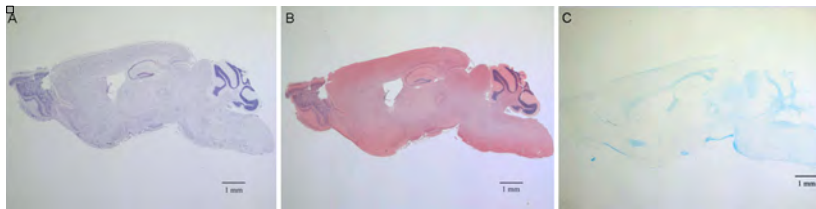

Figure 2. Unprocessed photomicrographs of adjacent sagittal (A) cresyl violet-, (B) hematoxylin and eosin-, and (C) luxol fast blue-stained sections of a 3 month old N3 WT C57BL/6 x 129/Sv male mouse.

2.2   Image processing, alignment, and anatomical identification

Photomicrographs were imported into Adobe Photoshop CS5 as .tif files (Figure 3A). The slide backgrounds were removed using the magnetic lasso tool to identify exterior of the cresyl violet-stained tissue (Figure 3B). Each section was concatenated as individual layers into a single .psd document. Images were aligned as follows: Sagittal alignments began with the section at the hemispheric midpoint and proceeded laterally in both directions. Coronal alignments began at bregma and proceeded rostral to the olfactory bulbs or caudally to the cerebellum. Each section was centred, colour balanced where necessary, and processed in pairs. Only the base section and overlay of each pair were made visible in the dataset. The opacity of the overlaid section was changed to 50%, so that both sections could be seen. Using the 'free rotation' and 'nudge' tools, the transparent section was aligned with the previously registered section using both anatomical landmarks and, where visible, the small drill holes along the lateral and dorsal surfaces of the cortex made at time of sacrifice. Opacity was restored to 100%. The first guide image was made invisible and the subsequent section was aligned to its new base layer. Following alignment, six anatomical regions of interest, (1) corpus callosum, (2) striatum, (3) cortex, (4) ventricles, (5) dentate gyrus, and (6) hippocampal formation, were manually identified and outlined in Adobe Photoshop CS5 using the polygonal lasso tool. The hippocampal formation was further subdivided into (7) the CA fields of the hippocampus. The dentate gyrus was divided into (8) the granule cell layer of the dentate gyrus. The overall volume of the (9) exterior surface of the brain was outlined separately for each section. In total,

nine separate volumes have been mapped to date and rendered in 3D. Each outline was smoothed using the 'smooth' command, and traced by our teams' neuroanatomists using the 'stroke' command along accepted anatomical borders identifiable by cresyl violet staining. A line thickness of two pixels was used. Each structure and subfield was traced as a separate layer (Figure 3C). 'Export layers to files' function was used to export individual files into Maya 2012 and for registration on a stereotaxic corresponding to the coordinate system of Paxinos and Franklin [7] (Figure 4).
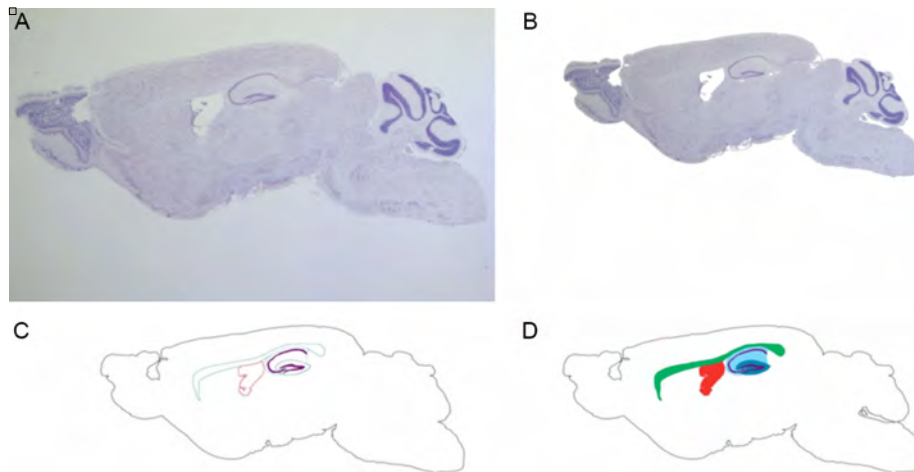

Figure 3. Image processing, anatomical tracing, and preparation for import into Maya 2012. (A) Raw image. (B) Background removal. (C) Anatomical tracing. (D) Solid object preparation (solid model of the exterior is not shown). Regions are colour-coded for import: Green, corpus callosum; red, ventricles; turquoise, hippocampus; violet, CA fields of the hippocampus; aquamarine, dentate gyrus; blue, granule layer of the dentate gyrus.

2.3   Creation of the 3D C57BL/6 and C57BL/6 x 129/Sv base models

Base models were created initially using solid objects of the anatomical tracings of each region identified in every 10th section (collected every 50 µm). Each outlined structure was filled using the paint bucket tool in Adobe Photoshop CS5 (Figure 3D). Solid objects were imported into Autodesk Maya 2012. Surface planes (slices) linked to each photomicrograph were created in the Maya workspace with the length-width ratio equal to the 3300 x 2550 pixel Photoshop files (Figure 5). The traced profiles were imported as Lambert materials and entered into the Maya workspace. Textures were made for each surface plane. Individual planes, made up of eight Lambert materials, were extruded to their final depth (5 µm) and successively shifted in space to reconstruct their spacing (every 50 µm). Each plane was renamed as a "Slice" and referenced to its original tissue section in an Excel spreadsheet (i.e., in the Slice _025 in Maya 2012 corresponds to 4160-Traced_0025_380.tif referencing the Photoshop
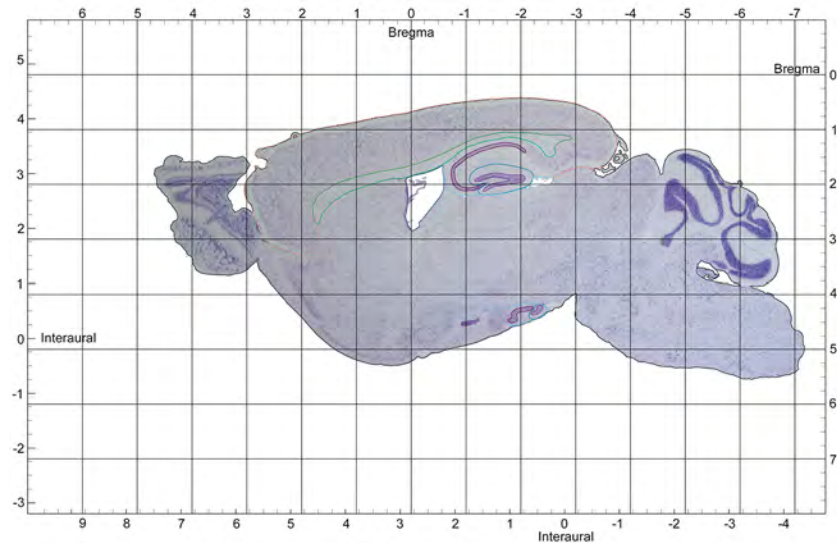
Figure 4. Creation of the 2D digital N3 C57BL/6 x 129/Sv atlas. Sagittal serial sections were registered on a stereotaxic grid with interaural and bregma coordinates indicated using the coordinate system corresponding to Paxinos and Franklin [7]. Tracings were colour-coded: green, corpus callosum; grey, ventricles; turquoise, hippocampus; violet, CA fields of the hippocampus; blue, dentate gyrus; magenta, granule layer of the dentate gyrus; brown, cortex.
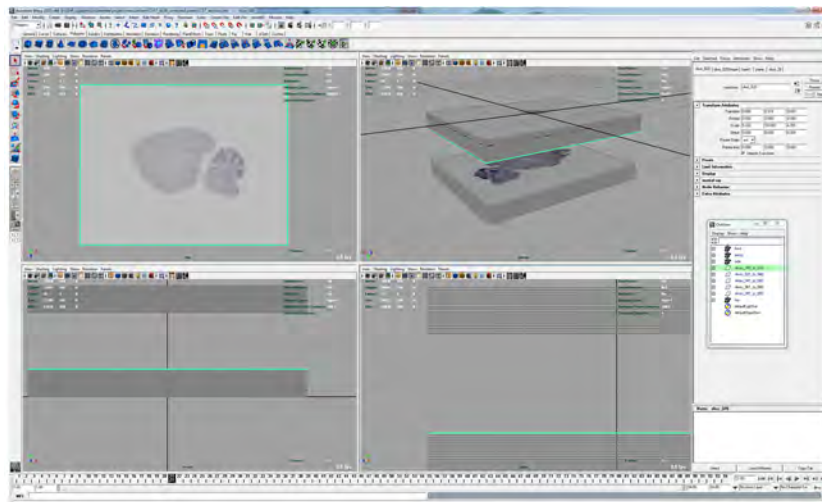

Figure 5. Layout of planes in the base models created in Maya 2012. The timeline frame is set to 21 (Bottom left panel, green) and the 20th plane (Slice_20) is shown (Top left panel, green). In the outliner window, the orientations of 5 planes, grouped with Slice_20, are represented (Top right panel). Only "slices_000_to_020" and "slices_061_to_080" are set to visible in this example with the active slice_20 indicated in green (Bottom right panel).

file with animal number (4160), Maya plane (0025), and section number (380)). The planes were further grouped into 5 planes per group based on location to facilitate regional manipulation (Figure 5). In the texture's attribute window, a colour was applied to each individual structure across planes. To facilitate spatial analysis, the Maya timeline function was adapted such that each timeline frame was indicative of a 50 μm increment in space (Figure 5). To display frames of each structure within these 50 μm divisions, the Top view was selected and its attribute window opened. At one second, the Top views' Near and Far Clip Planes were keyed so that only the first plane (Slice_00) was visible. The same was done for the last frame. Because planes start at 00 but the timeline begins at one, each plane is visible at the frame one higher than itself – i.e. Slice_05 is visible at Frame 6. Once the overall structures were modelled at regular 50 μm intervals, additional sections were inserted according to their registered position. These intermediate sections were imported using only the traced element without solid infill. For each section, within the Hypershade window of Maya, a new Lambert surface was created and renamed appropriately according to position, i.e., Slice_25. Thus, as one moves through the timeline, all planes inserted within a given 50 μm interval (frame) are displayed when set to visible (Figure 5).

2.4   Creating the anatomical volumes

Following creation of the planes, each anatomical structure was modeled as a single object (per hemisphere) by repeatedly extruding one or more cubes until anatomical form was recapitulated. Start and end planes were first identified for each structure. Where required, complex structures were "blocked" into multiple cubes. An example of this process is presented in Figure 6. Here, the dentate gyrus in the left cerebral hemisphere was first apparent in the 4th plane (slice_04). By the 18th plane, the structure could be seen to split into dorsal and ventral subdivisions, extending to the 45th and 31st planes respectively. To address this change in form, a cube was positioned encompassing the maximal area of the dentate gyrus before its bifurcation (Figure 6A). Using the snaps, the original cube was then moved to its starting plane and the bottom four vertices fixed (i.e., on the 4th plane or slice_04). Its top four vertices were extruded through the planes immediately above. In the example provided, the cube's upper vertices can be seen in the process of extrusion from the 4th plane (slice_04) through to the top of 6th plane (slice_06) (Figure 6B). This was repeated until the cube had been extruded to the plane immediately lateral (posterior in the construction orientation) to the point of bifurcation into dorsal and ventral structures (slice_17). Using the "split polygon tool" (polygons>edit mesh>split polygon), the initial cube's face was split into two separate volumes (Figure 6C). Each volume was then extruded separately until the end of the each substructure (dorsal and ventral regions) was reached. The area of these new cubes were scaled to adjust for the different sizes of the dorsal and ventral aspects of the dentate gyrus at these spatial locations. Initially, these cubes did not completely encompass the x and y profiles of new volumes. Only the z axis was considered once the cubes were split in two (Figure 6D). This was done to ensure no gap in the complete volume along the z axis. Fine adjustments were made in the next modeling step.
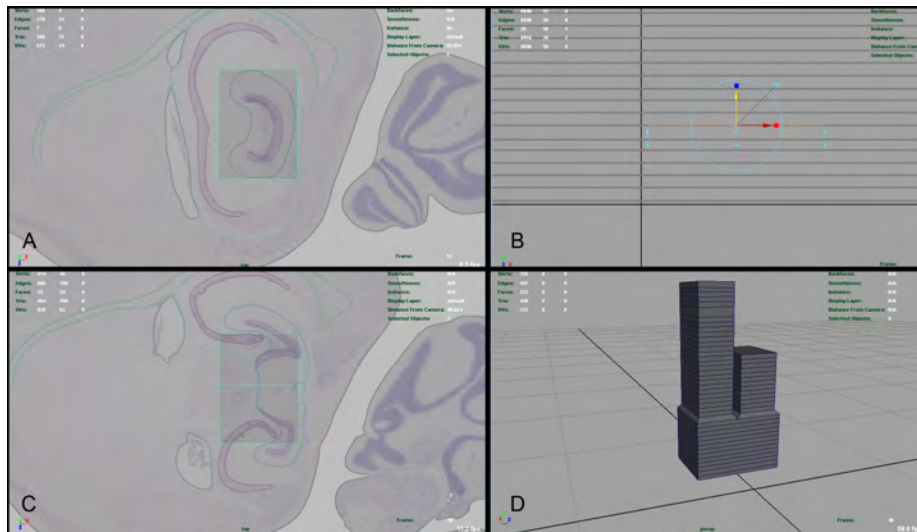
Figure 6. Modeling each anatomical structure. The process of creating the initial cubes for the dentate gyrus is depicted. (A) A cube was made at the approximate maximal size of the structure prior to point of bifurcation. (B) The base was moved to the starting plane at which the dentate gyrus was first apparent. The top was extruded repeatedly through each plane until slice_17 (17th plane), just prior to the bifurcation of the dentate gyrus into dorsal and ventral substructures, was reached. (C) At the 17th plane, the top face was split into two faces. (D) Both faces were extruded until they encompassed the entire structure.

Once the volumetric cubes were established, they were transformed into gross forms that approximated the structures of interest, and then fine-tuned, to recapitulate the 2D anatomical tracings. Figure 7 depicts this process for the hippocampus (left hemisphere). The four vertices of the structure-defined cube were placed at the four most distal points of the anatomical profile on the base plain. The timeline was then moved through each 50 μm frame and the four vertices in each frame were placed at the four edges of the maximal profile line in each 3D position. Once the gross form was approximated, additional vertices were added to model the curves present in each profile (Figure 7A). The selection mode was switched to "edge." An edge was selected. Using the "add divisions" tool (polygons>edit mesh>add divisions), as many vertices as necessary were added to model the hippocampal contours in each plane. As needed, vertical edges between planes were added to smooth approximate final volume in 3D space using the "interactive split tool" in Maya 2012 (Figure 7B).

2.5   Refining the anatomical volumes manually

Four experimental errors contributed to artefacts in the 3D volumes and required manual correction in the modelling stage. First, we noted that subtle changes in the angle of the microtome blade over the course of sectioning affected the orientation of groups of sections. Ideally, brains are serially sectioned in one sitting, thus cut at the same angle from beginning to end. However, did not perform 24 h sectioning as has been recently used to section the brain of the famous amnesiatic patient Henry G.
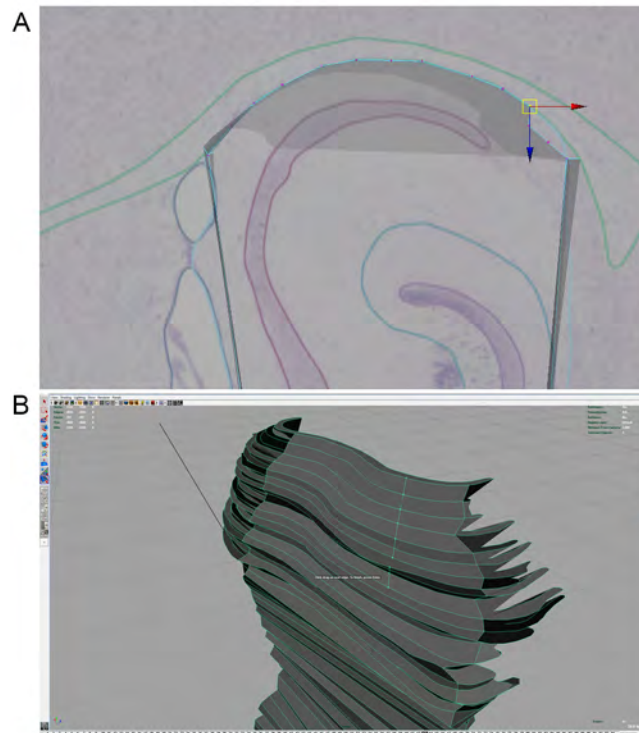
Figure 7. Refining the profile of each anatomical structure. (A) In each plane, the cubes were altered to approximate the gross form moving the four initial vertices to the distal edges of each profile. Additional edge vertices were added as needed to delineate curvilinear shapes. (B) Vertical extrusions between planes were used closed gaps along the Z axis.

Molaison (H.M.) [15, 16]. In our study, each brain was serially sectioned over a 72-168 h period with 2-3 breaks in cutting per day. Although the paraffin blocks were never removed from the microtome chuck, expansion of the blocks occurred each time the paraffin was ice-chilled at the start of a new session. The expansion and contraction were predicted to alter the angle of the microtome blade entering the block at the beginning of each session. Consistent with this hypothesis, we identified a progressive skew in the 3D model when the planes/slices were entered successively at the same angle (Figure 8A). To correct this, each group of planes per session were manually reoriented at an angle that aligned them relative to the original cut angle of the first session (Figure 8B). Second, because the profile of each anatomical volume was manually traced by one of three expert anatomists, we found that minor discrepancies between the volumetric tracings of adjacent sections created artificial "bumps" in the 3D volumes that required smoothing where the sections were geometrically inconsistent (Figure 9A,B). Third, in rare frames, a single plane was occasionally offset. These offsets were readily apparent and easily corrected once entire anatomical volumes were completed. Fourth, the floating, mounting, and drying process of the paraffin sections onto the microscope slides resulted in minor stretching in the X or Y dimension of some sections. This was exemplified in the "wave" effect
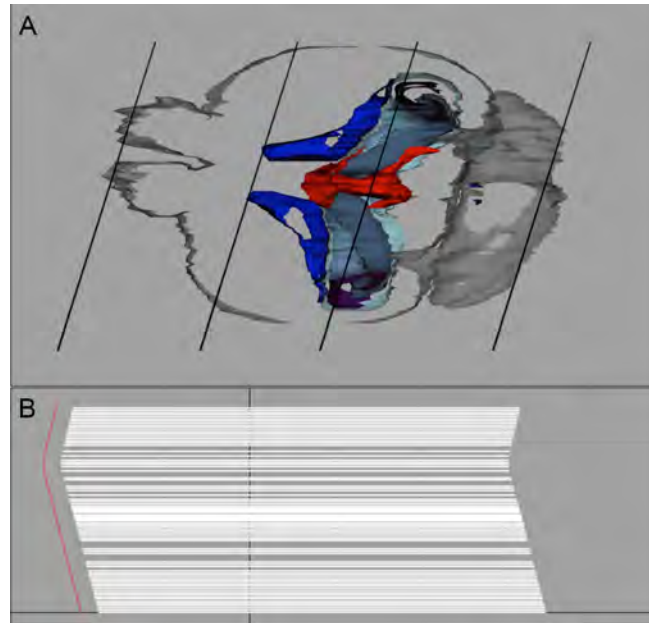
Figure 8. Expansion and contraction artefacts. (A) A tangential view of the 3D model through the centre of the brain reveals the progressive skew evident when sections are entered on the same plane in Maya 2012. (B) Examples of the realignments required in groups of planes to adjust for these changes in the angle of the microtome blade at the start of each session.
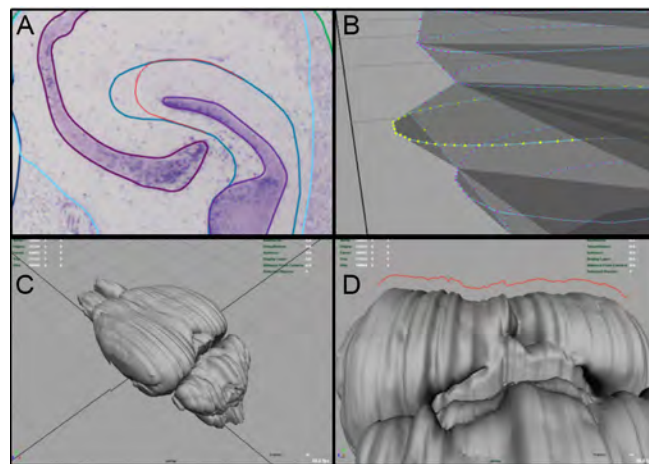

Figure 9. Processing and registration artefacts requiring manual correction in the 3D models. (A) Minor variations in the identification and registration of anatomical structures in successive sections (dentate gyrus: blue and red) manifested as (B) marked vertical deviations (yellow) between triads of successive slices/planes (blue-yellow-blue). (C) Minor variations in the exterior surface also appeared as series of undulations in the surface volume. (D) These slight deviations were identified (red) and smoothed (see Figure 10 for final result).

observed in reconstructions of the exterior surface of each structure, most prominent on the surface of the brain itself (Figure 9C,D). Here, addition of vertical edges in the final rendition were used to correct and smooth these processing artefacts. To ensure accuracy, the final models were compared to digital documentation of the exterior surface of the brain prior to paraffin embedding. Following all manual corrections, the "split polygon tool" was employed creating a more complex surface. Each anatomical volume was then selected and smoothed using the "Smooth" tool (polygons>mesh>smooth). All manual corrections were made in consensus between one of our teams' Maya modellers and one of our neuroanatomists. We found that, because the exterior surface of the brain exhibited the most deformation attributed to section mounting, smoothing alone was not sufficient. We used the "Sculpt Geometry tool" (polygons>mesh>sculpt geometry tool) only on the exterior surface. To minimize automatic smoothing, under "Brush and radius to an appropriate size," "Accumulate Opacity" was not checked. The "Smooth" brush was selected and applied to undulating areas of the volume until the desired smoothness was achieved.

2.6   Rendering the final models

Scenes and volumes were established in Maya 2012 and models were rendered on 16 Microsoft server blades controlled by a central HS20 with 2 Xeon 3.06GHz/533MHz processors and 4.5GB RAM. The final product is presented in Figure 10. Animations of these 3D models are freely available at http://neurolipidomics.com/resources.html.

3   Validation and analysis

To validate these 2D and 3D models and assess inter-animal variability in neuroanatomical organization, we measured the length, width, and volume of seven anatomical structures n=4 animals per strain and we used stereotaxic injections of the retrograde tracer fluorogold in n=5-6 animals per strain to establish accuracy of our alignments comparing to established 2D and 3D atlases of inbred lines [1, 5, 6, 12, 13].

3.1   Maximal length and width of the N3 C57BL/6 x 129/Sv cerebrum compared to donor (129/Sv) and recipient (C57BL/6) lines

The length from posterior end of olfactory bulb to anterior position of cerebellum was calculated in mm for each C57BL/6, 129/Sv, and N3 C57BL/6 x 129/Sv brain (n=4). The width of each brain was determined by summing each section volume (5 μm) in the sum of all serial sagittal sections, taking into consideration sections not collected. 129/Sv mice are known to have a wider and longer cerebrum than C57BL/6 mice [1] replicated here (Figure 11A,B). N3 hybrid mice were found to exhibit an intermediate phenotype with features of both donor and recipient lines. Cerebrums were significantly shorter than 129/Sv but wider than C57BL/6 mice (Figure 11A,B).
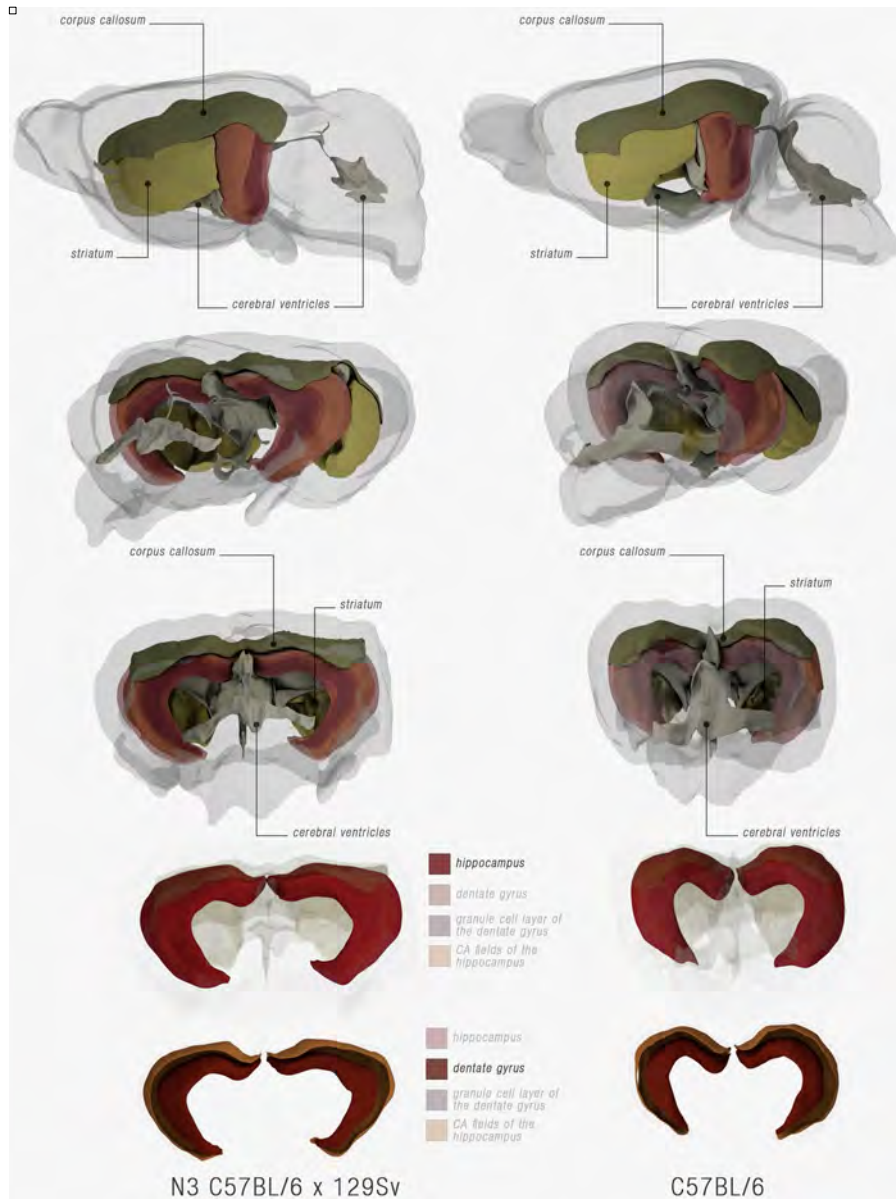
Figure 10. 3D reconstructions in Autodesk Maya of anatomical regions of interest in the N3 C57BL/6 x 129Sv and C57BL/6 mouse brain.

3.2   Quantitation of anatomical volumes

Volumes were measured using the 'advanced measurement module' of OpenLab 5.0 calibrated in μm and using the Cavalieri stereological principle [17, 18]. The

volume of each section was determined by multiplying the cross-sectional area by the distance between consecutive sections and then summing consecutive volumes within this range. Only the lateral ventricles exhibited strain-dependent differences in total volume. N3 C57BL/6 x 129/Sv mice exhibited an intermediate ventricular volume, significantly smaller than C57BL/6 mice but larger than 129/Sv lines (Figure 11C).
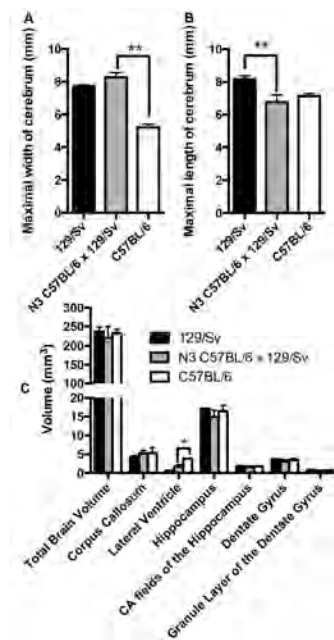

Figure 11. Quantitation of anatomical structures in the 2D and 3D models. (A) N3 hybrid mice have a wider cerebrum than C57BL/6 mice that is comparable to 129/Sv mice (n=4 per group). (B) Cerebrum length is significantly less in N3 hybrids than 129/Sv mice but comparable to C57BL/6 mice. (C) Overall volumes of multiple structures were comparable with the exception of the lateral ventricles. Ventricular volumes were largest in the C57BL/6 line and smallest in 129/Sv strains. N3 hybrid mice exhibited an intermediate phenotype, with volumes significantly smaller than C57BL/6 mice. Data are presented as mean $\pm$ standard error of measurement (SEM). Statistics were one-way ANOVA followed by post hoc Dunnett's comparing the structural volumes of each N3 C57BL/6 x 129/Sv hybrid line control group to both donor and recipient lines. * $p<0.05$, ** $p<0.01$.

3.3   Validation of the 2D and 3D spatial relationships in cerebral architecture represented in these N3 atlases by stereotaxic surgery

Taken together, these data suggest that, while overall volumes are consistent between all three mouse lines, positioning of neuroanatomical structures in x,y,z stereotaxic coordinates (Figure 10) is markedly different as has already been shown for C57BL/6 and 129/Sv inbred lines [1]. These differences are predicted to affect studies that require cerebral injection to deliver drug or viral and tracer cell tracking agents. To validate the utility of our N3 C57BL6 x 129/Sv 2D and 3D models in facilitating these studies, we injected the retrograde tracer fluorogold into the CA3c field of the hippocampus of 129/Sv, N3 C57BL/6 x 129/Sv, and C57BL/6 mice using the coordinates of Hof et al., [1] (129/Sv and C57BL/6) or coordinates established for N3 hybrid mice using our 2D and 3D atlas (Table 1).

Under halothane anesthesia, animals (n=5-6 per group) were placed into a stereotaxic grid. The dorsal surface of the skull was exposed with a single incision. The delivery needle was adjusted to appropriate anterior/posterior and medial/lateral positions. Point of entry into the skull was marked and a Dremel tool was used to make a single entry point through the skull without damaging tissue below. The needle was

Strain	Target (from Bregma in mm)			Reference Atlas
	A / P	M / L	D / V	
C57BL/6	-1.6	1.1	2.2	[1]
N3 Hybrid	- 1.9	0.9	2.2	*this study*
129/Sv	- 1.9	2.0	2.2	[1]

Table 1. Coordinates used for stereotaxic injections into the CA3c pyramidal cell field of the hippocampus for atlas validation. A/P, anterior/posterior; M/L, medial/lateral , D/V, dorsal ventral.

lowered through the entry hole to the required dorsal/ventral position. Once in position, an automated pump injected 1 μl of a 4% fluorogold solution (Fluorochrome, LLC, Denver, CO, USA) prepared in 10 mM PBS at a flow rate of 0.5 μl/min. The needle was then left in place for two minutes. Following withdrawal, the burr hole was filled with surgical glue and the incision closed with wound clips. Buprenorphine (Chiron Compounding Pharmacy Inc) was prepared in sterile water to a final concentration of 0.03 mg/ml. Mice received three injections (0.05 mg/kg, s.c.) of analgesic every 6 h on the day of surgery and one injection (0.05 mg/kg, s.c.) the following day as pain management. Mice were sacrificed 24 h after injection as described above. Injection sites were established in serial cryosections under epifluorescence using a Leica DMXR microscope.

We found that the accuracy of our surgeries using our N3 C57BL/6 x 129/Sv atlas, to target the the CA3c hippocampal field, was equivalent to those using established resources for inbred C57BL/6 and 129/Sv mice [1] (Figure 12). All surgeries were performed by the same surgeon. Variation in surgical accuracy was comparable
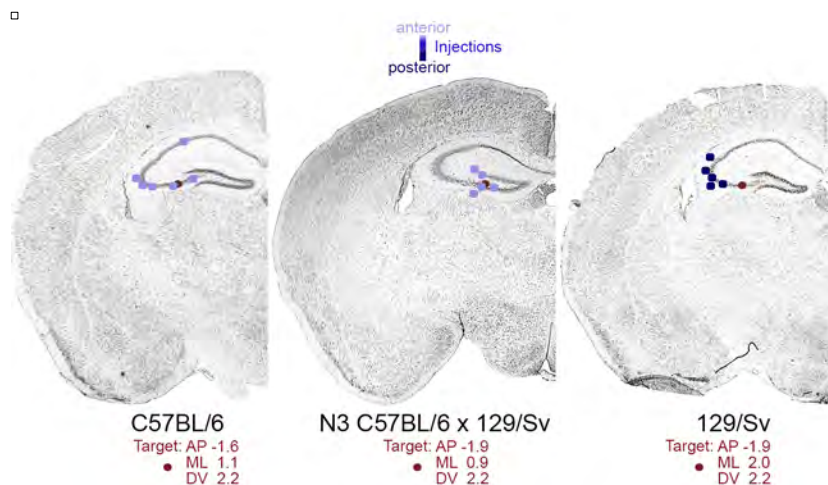
Figure 12. Stereotaxic validation of the accuracy of the N3 atlas. The positions of the fluorogold injection sites (blue) targeting the CA3c field of the hippocampus (red) using the coordinates of Hof et al [1] for C56BL/6 or 129/Sv inbred lines or our N3 C56BL/6 x 129/Sv prototype atlas are indicated. Coronal sections are shown. Injections that fell anterior (light blue) or posterior (dark blue) to the intended anterior/posterior position are colour coded. A total of 16 animals were analyzed (n=5 N3 or 129/Sv and n=6 C57BL/6).

Strain	Deviation from Target (mm)			Reference Atlas
	A / P	M / L	D / V	
C57BL/6	-0.18 + 0.04 n=6	-0.33 + 0.17 n=6	-0.31 + 0.15 n=6	[1]
N3 Hybrid	-0.31 + 0.25 n=5	-0.08 + 0.13 n=5	-0.18 + 0.14 n=5	*this study*
129/Sv	0.68 + 0.02 n=5	-0.54 + 0.11 n=5	0.26 + 0.15 n=5	[1]

Table 2. Deviation in x,y,z positioning of stereotaxic injections into the CA3c pyramidal cell field of the hippocampus. Data represent mean + SEM. A/P, anterior/posterior; M/L, medial/lateral , D/V, dorsal ventral.

between lines. In fact, in the N3 surgeries, variability in injection positioning was less than and accuracy/proximity to target was closer than those achieved by the same surgeon for either the C57BL/6 or 129/Sv (Table 2). We suggest that the refinements to the 2D atlas made as a result of the errors detected on 3D reconstruction significantly improved the accuracy of the reference atlas. Moreover, we were surprised to find that the anatomy of the filial offspring in the hybrid line were so reproducible suggesting that anatomical references can be accurately modelled not only for inbred mice but also for hybrid, incipient congenic, and congenic strains. We suggest that these resources will substantively assist researchers in minimizing unnecessary breeding and facilitate earlier analysis of their mouse models with greater accuracy.

4   Conclusion

In summary, we show that 3D modeling can be used to accurately depict the differences in cytoarchitecture between inbred and transgenic strains of mice. Furthermore, we show that the brains and subregions of N3, C57BL/6 and 129/Sv mice do not differ in total volume but exhibit significant differences in overall morphology in 3D space. These morphological differences are highlighted in our 3D model, 2D digital atlas, and can be adapted to map changes in "omic" datasets following injury.

5   Acknowledgements

McDowell, and Dr Hongbin Xu for critical reading and discussion.

6   References

1.   Hof, P.R., Young,W.G., Bloom, F.E., Belichenko,P.V., Celio, M.R. (ed.): Comparative Cytoarchitectonic Atlas of the C57BL/6 and 129/Sv Mouse Brains. Elsevier Science, London, UK (2001)

2.   Linder, C.C.: The influence of genetic background on spontaneous and genetically engineered mouse models of complex diseases. Lab animal 30, 34-39 (2001)

3.   Mott, R., Flint, J.: Dissecting quantitative traits in mice. Annual review of genomics and human genetics 14, 421-439 (2013)

4.   Jax Mice and Services - Mouse strain nomenclature tutorial. Available: http://jaxmice.jax.org/support/nomenclature/tutorial.html (2014)

5.   Franklin, K.B.J., Paxinos, G.T.: The Mouse Brain in Stereotaxix Coordinates. Academic Press, New York (2007)

6.   Sidman, R.L., Angevine, J.B., Pierce, E.T.: Atlas of the mouse brain and spinal cord. Harvard University Press, Cambridge (1971)

7.   Paxinos, G., Franklin, K.B.J.: Paxinos and Franklin's the Mouse Brain in Stereotaxic Coordinates. Elsevier Academic Press (2012)

8.   Manis, J.P.: Knock out, knock in, knock down--genetically manipulated mice and the Nobel Prize. N Engl J Med 357, 2426-2429 (2007)

9.   Fowler, C.D., Kenny, P.J.: Utility of genetically modified mice for understanding the neurobiology of substance use disorders. Human genetics 131, 941-957 (2012)

10.   Moore, C.B., Guthrie, E.H., Huang, M.T., Taxman, D.J.: Short hairpin RNA (shRNA): design, delivery, and assessment of gene knockdown. Methods Mol Biol 629, 141-158 (2010)

11.   Limaye, A., Hall, B., Kulkarni, A.B.: Manipulation of mouse embryonic stem cells for knockout mouse production. Current protocols in cell biology / editorial board, Juan S. Bonifacino ... [et al.] Chapter 19, Unit 19 13 19 13 11-24 (2009)

12.   Sunkin, S.M., Ng, L., Lau, C., Dolbeare, T., Gilbert, T.L., Thompson, C.L., Hawrylycz, M., Dang, C.: Allen Brain Atlas: an integrated spatio-temporal portal for exploring the central nervous system. Nucleic acids research 41, D996-D1008 (2013)

13.   Okamura-Oho, Y., Shimokawa, K., Takemoto, S., Hirakiyama, A., Nakamura, S., Tsujimura, Y., Nishimura, M., Kasukawa, T., Masumoto, K.H., Nikaido, I., Shigeyoshi, Y., Ueda, H.R., Song, G., Gee, J., Himeno, R., Yokota, H.: Transcriptome tomography for brain analysis in the web-accessible anatomical space. PLoS One 7, e45373 (2012)

14.   Deans, M.R., Gibson, J.R., Sellitto, C., Connors, B.W., Paul, D.L.: Synchronous activity of inhibitory networks in neocortex requires electrical synapses containing connexin36. Neuron 31, 477-485 (2001)

15.   Annese, J., Schenker-Ahmed, N.M., Bartsch, H., Maechler, P., Sheh, C., Thomas, N., Kayano, J., Ghatan, A., Bresler, N., Frosch, M.P., Klaming, R., Corkin, S.: Postmortem examination of patient H.M.'s brain based on histological sectioning and digital 3D reconstruction. Nature communications 5, 3122 (2014)
16.   Scoville, W.B., Milner, B.: Loss of recent memory after bilateral hippocampal lesions. J Neurol Neurosurg Psychiatry 20, 11-21 (1957)
17.   Mayhew, T.M., Olsen, D.R.: Magnetic resonance imaging (MRI) and model-free estimates of brain volume determined using the Cavalieri principle. Journal of anatomy 178, 133-144 (1991)
18.   Roberts, N., Cruz-Orive, L.M., Bourne, M., Herfkens, R.J., Karwoski, R.A., Whitehouse, G.H.: Analysis of cardiac function by MRI and stereology. Journal of microscopy 187, 31-42 (1997)